

# Astrophysical constraints for Scalar-Tensor-Vector Gravity based on Kerr black holes and jets

Federico G. Lopez Armengol,<sup>1\*</sup> Gustavo E. Romero,<sup>1,2</sup>

<sup>1</sup>*Instituto Argentino de Radioastronomía (CCT-La Plata, CONICET; CICPBA), C.C. No. 5, 1894, Villa Elisa, Argentina.*

<sup>2</sup>*Facultad de Ciencias Astronómicas y Geofísicas, Universidad Nacional de La Plata, Paseo del Bosque s/n, 1900 La Plata, Buenos Aires, Argentina.*

Accepted XXX. Received YYY; in original form ZZZ

## ABSTRACT

Scalar-Tensor-Vector Gravity (STVG), also referred as MODified Gravity (MOG), is an alternative theory for the gravitational interaction. Its weak field approximation has been successfully used to describe Solar System observations, galaxy rotation curves, dynamics of clusters of galaxies, and cosmological data, without the imposition of dark components. The theory was formulated by John Moffat in 2006. In this work we study the STVG-Kerr geometry, and the fields on it. In order to constrain free parameters of the theory, we model the black hole in the giant elliptical galaxy M87 and compare some predictions of STVG with observations. Further, we investigate the trajectories of particles in the relativistic jet of M87. We conclude that, according to STVG, gravity might play a significant role in the acceleration, collimation, and rotation of relativistic jets.

**Key words:** Gravitation – Black hole physics – Galaxies: jets

## 1 INTRODUCTION

It is nearly eighty years since the publication by Babcock (1939) noticing the discrepancies between galactic observations of rotation curves and gravitational theoretical predictions. Mainstream solutions to this problem have assumed the existence of some kind of dark matter. However, every experiment aimed at measuring the properties of such matter has failed (e.g. Aprile et al. 2012; LUX Collaboration et al. 2013; Agnese et al. 2014). In this context, alternative solutions involving modifications of fundamental physical laws deserve some attention.

In 1983, Milgrom (1983) proposed the MODified Newtonian Dynamics theory (MOND) to account for astrophysical gravitational phenomena without dark matter. Several relativistic theories whose weak field limit is coincident with MOND were soon formulated. For a review of MOND predictions and its relativistic extensions, see Famaey & McGaugh (2012). Motivated by some problems of these extensions, Moffat (2006) postulated the Scalar-Tensor-Vector Gravity theory (STVG), also referred as MODified Gravity (MOG) in the literature.

In STVG, the gravitational coupling constant  $G$  is reified to a scalar field whose numerical value usually exceeds Newton's constant  $G_N$ . This assumption serves to describe

correctly galaxy rotation curves (Brownstein & Moffat 2006), cluster dynamics (Moffat & Rahvar 2014), Bullet Cluster phenomena (Brownstein & Moffat 2007), and cosmological data (Moffat & Toth 2007), without requiring the existence of dark contributions. In order to counteract the enhanced gravitational coupling constant on Solar System scales, Moffat proposed a gravitational repulsive Yukawa-like vector field  $\phi^\mu$ . In this way, Newton's gravitational constant can be retrieved and STVG coincides with General Relativity (GR), for instance, in the Solar System.

The interplay between enhanced attraction and repulsion can be seen from the radial acceleration of a particle in the weak field, static, spherically symmetric approximation with constant scalar fields (see Moffat 2006):

$$a(r) = -\frac{G_N(1+\alpha)M}{r^2} + \frac{G_N\alpha M}{r^2}e^{-\tilde{\mu}r}(1+\tilde{\mu}r), \quad (1)$$

where we adopted natural units,  $M$  denotes the gravitational mass source,  $r$  the distance from it,  $G_N$  is Newton's gravitational constant, and  $\alpha, m$  are free parameters of the theory. The first term of Eq. (1) prevails at  $r \rightarrow \infty$ , and represents an enhanced (as compared to GR) gravitational attraction, quantified by  $G_\infty = G_N(1+\alpha)$ . As mentioned, such term describes correctly galaxy rotation curves, light bending phenomena, and cosmological data, without dark matter. The second term is significant when  $\tilde{\mu}r \ll 1$  and represents gravitational repulsion. Such Yukawa-type force counteracts

\* E-mail: flopezar@iar-conicet.gov.ar

the enhanced attraction allowing Newton gravitational constant to arise on the right scale.

According to Eq. (1) the difference between STVG and GR manifests solely far from the gravitational source, where phenomena usually related with dark matter happen. However, Eq. (1) is based on several assumptions that may fail in the strong field regime. In this work we study the predictions of both theories in such regime, to find out whether STVG deviates from GR on shorter scales as well. Specifically, we investigate the geodetic deviation of test particles close to a STVG-Kerr black hole.

Black hole solutions of STVG field equations can be found in Moffat (2015). Such solutions formally resemble the electrically charged and rotating black holes of GR. For this reason, we expect to find effects of gravitational Lorentz-like forces on the movement of particles around STVG-Kerr black holes. This would imply the existence of novel observable differences between STVG and GR.

Relativistic jets launched from the surroundings of supermassive black holes in active galactic nuclei (AGNs) are expected to be sensitive to these Lorentz-like gravitational forces. This is because the launching region is located near the event horizon, where strong field effects are important, and because the relativistic velocities involved in the propagation of matter.

In the case of nearby sources, collimation, bending, and structural effects of the gravitational field on the jet might be observationally detectable and then used to test the adopted background field theory. Particularly, the extragalactic jet of the giant elliptical galaxy M87 (a.k.a. Virgo A, NGV4486, and 3C274) has been resolved up to 100 gravitational radii using Very Long Baseline Interferometry (VLBI), see Mertens et al. (2016). This, along with the fact that from mm-VLBI observations there are constraints on the size of M87 supermassive black hole (hereafter M87\*) (see Broderick et al. 2015), might provide a unique scenario to test some predictions of STVG.

In this work we model M87\* phenomena in order to set new restrictions on the free parameters of STVG theory. Our work is organized as follows: in Section 2 we present the action and field equations of STVG, along with certain simplifications adopted. In Section 3 we describe the STVG-Kerr geometry, we find the equations of motion for test particles, and characterize a set of trajectories called *vortical orbits*. Then, in Section 4 we present a numerical code developed for integrating such equations for a particle in the jet. Section 5 is devoted to our main results about particle motion in STVG, for different sets of initial conditions, and the parameters  $\alpha$  and  $\kappa$  of the theory. In Section 6 we present some discussion about the application of our results to jet phenomenology. Finally, in Section 7 we state our conclusions.

## 2 STVG ACTION AND FIELD EQUATIONS

STVG action reads<sup>1</sup>:

$$S = S_{\text{GR}} + S_{\phi} + S_S + S_M, \quad (2)$$

where

$$S_{\text{GR}} = \frac{1}{16\pi} \int d^4x \sqrt{-g} \frac{1}{G} R, \quad (3)$$

$$S_{\phi} = - \int d^4x \sqrt{-g} \left( \frac{1}{4} B^{\mu\nu} B_{\mu\nu} - \frac{1}{2} \tilde{\mu}^2 \phi^\mu \phi_\mu \right), \quad (4)$$

$$S_S = \int d^4x \sqrt{-g} \left[ \frac{1}{G^3} \left( \frac{1}{2} g^{\mu\nu} \nabla_\mu G \nabla_\nu G - V(G) \right) + \frac{1}{G \tilde{\mu}^2} \left( \frac{1}{2} g^{\mu\nu} \nabla_\mu \tilde{\mu} \nabla_\nu \tilde{\mu} - V(\tilde{\mu}) \right) \right]. \quad (5)$$

Here,  $g_{\mu\nu}$  denotes the spacetime metric,  $R$  is the Ricci scalar, and  $\nabla_\mu$  the covariant derivative;  $\phi^\mu$  denotes a Proca-type massive vector field,  $\tilde{\mu}$  is its mass, and  $B_{\mu\nu} = \partial_\mu \phi_\nu - \partial_\nu \phi_\mu$ ;  $V(G)$  and  $V(\tilde{\mu})$  denote possible potentials for the scalar fields  $G(x)$  and  $\tilde{\mu}(x)$ , respectively. We adopt the metric signature  $\eta_{\mu\nu} = \text{diag}(-1, 1, 1, 1)$  and natural units. The term  $S_M$  in the action refers to possible matter sources.

We adopt certain simplifications on the action. First, we neglect the mass of the vector field  $\phi^\mu$  because its effects manifest at kiloparsec scales from the source and here we are interested in the sub-parsec jet. This means that we are not considering the decay of the Yukawa-type force on such scale. The same approximation has been made in Moffat (2015) and Hussain & Jamil (2015). Second, we approximate the scalar field  $G$  as a constant and adopt the same prescription as Moffat (2006):

$$G_\infty = G_N(1 + \alpha), \quad (6)$$

where  $\alpha$  is a free parameter whose value we will sample. Finally, we nullify the matter action term  $S_M$  because we study a vacuum black hole spacetime. The simplified action takes the form:

$$S = \int d^4x \sqrt{-g} \left[ \frac{1}{16\pi G_\infty} R - \frac{1}{4} B^{\mu\nu} B_{\mu\nu} \right], \quad (7)$$

which formally resembles the Einstein-Maxwell action. Despite this formal resemblance, we emphasize that there is no electric charge involved in the STVG spacetime we are studying.

From action (7), we get the dynamical equations of the theory. By varying with respect to the metric  $g^{\mu\nu}$  we obtain:

$$G_{\mu\nu} = 8\pi G_\infty T_{\mu\nu}^\phi, \quad (8)$$

where  $G_{\mu\nu}$  denotes the Einstein tensor, and

$$\begin{aligned} T_{\mu\nu}^\phi &= - \frac{2}{\sqrt{-g}} \frac{\delta S_\phi}{\delta g^{\mu\nu}} = \\ &= \left( B_\mu{}^\alpha B_{\nu\alpha} - g_{\mu\nu} \frac{1}{4} B^{\rho\sigma} B_{\rho\sigma} \right). \end{aligned} \quad (9)$$

<sup>1</sup> Compared with Moffat (2006) original action, we drop the cosmological constant term because its effects are locally negligible. We also ignore the scalar field  $\omega$  as suggested by Moffat & Rahvar (2013), and we set the potential  $W(\phi) = 0$  (Moffat 2006).

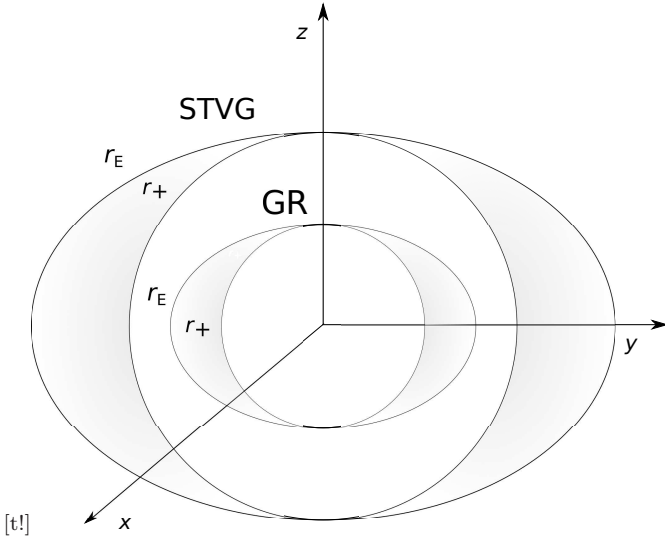


**Figure 1.** Scheme of STVG-Kerr and GR-Kerr geometrical structures in Kerr-Schild “Cartesian” coordinates  $(x, y, z)$ . The surface defined by  $r = r_E$  is the ergosphere’s boundary. The ergosphere extends down to the first event horizon  $r = r_+$ . As Eqs. (15) and (16) determine, the ergosphere and outer event horizon surfaces for STVG black holes are larger than in GR for the same mass and positive  $\alpha$ .

Furthermore, varying the action (7) with respect to the vector field  $\phi_\mu$  yields:

$$\nabla_\nu B^{\nu\mu} = 0. \quad (10)$$

Finally, the equation of motion for a test particle in coordinates  $x^\mu$  is given by:

$$\left( \frac{d^2 x^\mu}{d\tau^2} + \Gamma_{\alpha\beta}^\mu \frac{dx^\alpha}{d\tau} \frac{dx^\beta}{d\tau} \right) = \frac{q}{m} B^\mu{}_\nu \frac{dx^\nu}{d\tau}, \quad (11)$$

where  $\tau$  denotes the particle proper time, and  $q$  the coupling constant with the vector field. We define here the parameter  $\kappa = q/m$ , whose value we will sample along with  $\alpha$ .

### 3 STVG-KERR SPACETIME

#### 3.1 Geometry

The vacuum and axially symmetric solution of the metric field equation (8) for a body with mass  $M$  and spin angular momentum per unit mass  $a$  has been given in Moffat (2015). In Boyer-Lindquist coordinates it reads:

$$ds^2 = -\frac{\Delta}{\rho^2} \left[ d(ct) - \frac{a \sin^2 \theta}{c} d\phi \right]^2 + \frac{\sin^2 \theta}{\rho^2} \left[ \left( r^2 + \frac{a^2}{c^2} \right) d\phi - \frac{a}{c} d(ct) \right]^2 + \frac{\rho^2}{\Delta} dr^2 + \rho^2 d\theta^2, \quad (12)$$

where

$$\Delta = r^2 - \frac{2G_\infty M}{c^2} r + \frac{a^2}{c^2} + \frac{G_N Q^2}{c^4}, \quad (13)$$

$$\rho^2 = r^2 + \frac{a^2}{c^2} \cos^2 \theta, \quad (14)$$

and  $Q = \sqrt{\alpha G_N} M$ . The value of  $Q$ , dependent on the parameter  $\alpha$  and the mass  $M$  of the black hole, determines the strength of the gravitational vector forces.

The black hole geometry (12) presents two horizons, given by the roots of  $\Delta = 0$ :

$$r_\pm = \frac{G_\infty M}{c^2} \left( 1 \pm \sqrt{1 - \frac{c^2 a^2}{G_\infty^2 M^2} - \frac{\alpha}{1 + \alpha}} \right), \quad (15)$$

and an ergosphere determined by the roots of  $g_{00} = 0$ :

$$r_E = \frac{G_\infty M}{c^2} \left( 1 \pm \sqrt{1 - \frac{c^2 a^2 \cos^2 \theta}{G_\infty^2 M^2} - \frac{\alpha}{1 + \alpha}} \right). \quad (16)$$

Furthermore, the spacetime is singular at  $\rho = 0$ , presenting the usual Kerr-Schild “Cartesian” ring singularity. In Fig. 1 we show a sketch of the STVG-Kerr spacetime and the corresponding black hole of the same mass in GR. STVG geometrical structures grows in size with  $\alpha$ . For instance, the outer event horizon of a STVG black hole is bigger than in GR for positive  $\alpha$ . We use of this fact to impose an upper bound on the value of  $\alpha$  based on mm-VLBI observations of the environs of M87\*. We turn now our attention to the gravitational vector field  $\phi^\mu$ . We have to solve Eq. (10) for the black hole spacetime (12). Such equation has been studied exhaustively in the context of Einstein-Maxwell theory, as can be seen, for instance, in Misner et al. (1973). The solution for STVG is given by:

$$\mathbf{B} = \frac{Q}{c\rho^4} (r^2 - a^2 \cos^2 \theta) d\mathbf{r} \wedge \left[ d\mathbf{t} - \frac{a}{c} \sin^2 \theta d\phi \right] + \frac{2Qa}{c^2 \rho^4} r \cos \theta \sin \theta d\theta \wedge \left[ \left( r^2 + \frac{a^2}{c^2} \right) d\phi - \frac{a}{c} d\mathbf{t} \right]. \quad (17)$$

Following Moffat’s idea, the radial gravito-electrical components  $B^{0i}$  counteracts the enhanced attraction of  $G_\infty$ . However, gravito-magnetic components  $B^{ij}$  give raise to novel gravitational forces. In Fig. 2 we show the vector maps of the vector field solution.

The gravitational field given by Eq. (17) can be derived from a vector potential in Boyer-Lindquist coordinates:

$$\mathbf{A} = -\frac{Qr}{\rho^2} (d\mathbf{t} - a \sin^2 \theta d\phi). \quad (18)$$

#### 3.2 Test particle equations of motion

Having specified the spacetime geometry and the fields on it, we proceed to study the trajectories of a test particle of mass  $m$  in Boyer-Lindquist coordinates. We have to solve the equations of motion (11), for the geometry (12) and field (17). Such equations of motion have been treated in the context of Einstein-Maxwell theory for the Kerr-Newman black hole, see Misner et al. (1973) and Carter (1968). Adapting such results for STVG trajectories, we find the following first order differential equations:

$$\rho^2 \frac{dr}{d\lambda} = \pm \sqrt{R(r)}, \quad (19)$$

$$\rho^2 \frac{d\theta}{d\lambda} = \pm \sqrt{\Theta(\theta)}, \quad (20)$$

$$\rho^2 \frac{d\phi}{d\lambda} = - \left( \frac{aE}{c^2} - \frac{a}{\sin^2 \theta} \right) + \frac{aP(r)}{\Delta(r)c^2}, \quad (21)$$

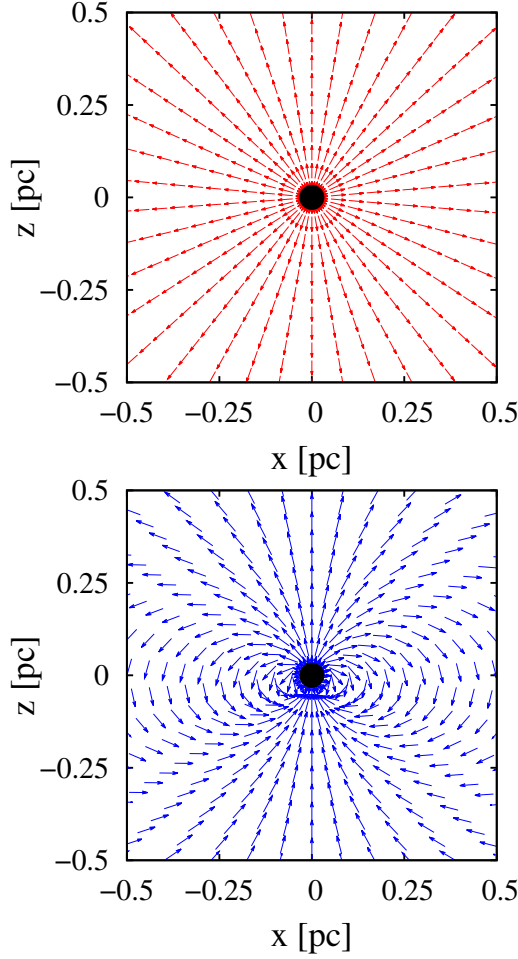


**Figure 2.** Vector maps of field  $B^{\mu\nu}$  on  $x-z$  plane of Kerr-Schild coordinates, generated by a supermassive black hole with mass  $M = 6 \times 10^9 M_\odot$ , and angular momentum  $a = 0.9 G_N M/c$ . The field lines are normalized. *Top:* Vector field map of gravito-electric components  $B^{0i}$ . These components are radial, and generate a gravitational repulsive force on neutral particles that counteracts the enforced attraction determined by  $G_\infty = G_N(1 + \alpha)$ . In the weak field limit, such mechanism serves to recover Newton gravitational law. *Bottom:* Vector field map of gravito-magnetic components  $B^{ij}$ . The field lines have the familiar disposition of a magnetic dipole, generated by a rotating charge. These components produce gravito-magnetic forces on particles. Such forces are completely absent in the formalism of GR.

$$\rho^2 \frac{dt}{d\lambda} = -\frac{a \sin^2 \theta}{c^2} \left( \frac{aE}{c^2} - \frac{L}{\sin^2 \theta} \right) + \left( r^2 + \frac{a^2}{c^2} \right) \frac{P(r)}{\Delta(r)c^2}, \quad (22)$$

where  $\lambda = \tau/m$ ,  $E$  stands for the particle energy, and  $L$  for its angular momentum around the symmetry axis; both  $E$  and  $L$  are constants of motion. Furthermore, we have the functions:

$$R(r) = \frac{P^2(r)}{c^2} - \Delta(r) (m^2 r^2 c^2 + \mathcal{K}), \quad (23)$$

$$\Theta(\theta) = \mathcal{Q} - \cos^2 \theta \left[ a^2 \left( m^2 - \frac{E^2}{c^4} \right) + \frac{L^2}{\sin^2 \theta} \right], \quad (24)$$

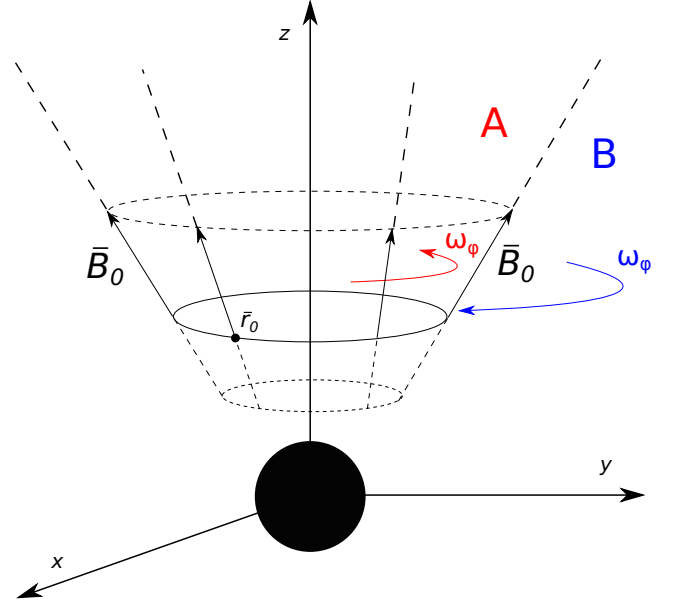


**Figure 3.** Scheme of STVG-Kerr black hole and the gravito-magnetic field  $B_0$  in the initial position  $r_0$  of a test particle. Because of  $\phi$  invariance, the gravito-magnetic field is the same for  $\phi$ -translated points. Such set of vectors defines the boundary of two regions called A and B in the figure. If the particle moves in region A, the Lorentz-like force contribute to  $\phi$  rotation. On the contrary, if the particle moves in region B, the Lorentz-like force will have opposite sign, contributing to  $-\phi$  rotation.

$$P(r) = E \left( r^2 + \frac{a^2}{c^2} \right) - aL - qQr, \quad (25)$$

where we make use of Carter constant of motion  $\mathcal{K}$ , and the combination of constants  $\mathcal{Q}$ :

$$\mathcal{K} = p_\theta^2 + \cos^2 \theta \left[ a^2 \left( m^2 - \frac{E^2}{c^4} \right) + \frac{L^2}{\sin^2 \theta} \right], \quad (26)$$

$$\mathcal{Q} = \mathcal{K} + \left( L - \frac{aE}{c^2} \right)^2. \quad (27)$$

In the next section we explain how to integrate numerically equations (19)-(22) for a relativistic particle in a jet centered along the rotation axis of the black hole. We expect to find differences with respect to GR in the motion along the coordinate  $\phi$ . This is because gravito-magnetic forces on particles ejected in the direction  $\check{z}$ , act along  $\check{\phi}$ . However, if the ejection angle is wide, these forces invert their direction towards  $-\check{\phi}$ . The dependence on the ejection angle follows from the usual vector product between the particle velocity and the magnetic-like field. In Figure 3 we sketch the physical system, distinguishing regions with positive and negative angular velocity  $\omega_\phi$ , as determined by the initial gravito-magnetic field.

### 3.3 Vortical orbits

The standard model for explaining the formation process of relativistic jets is based on magneto-centrifugal accelerated particles (see [Spruit 2010](#)). However, pure gravitational models also constitute an active line of research. In

de Felice & Calvani (1972) the authors studied the allowed ranges of variation for the coordinate  $\theta$  in the geodesics of Kerr spacetime. They found a set of geodesics for unbound particles, which they called *vortical orbits*, that spiral around the symmetry axis and never cross the equatorial plane. Further, in de Felice & Curir (1992), the authors showed that perturbing particular vortical orbits leads to collimation around the symmetry axis. For recent work of this line of research, see Gariel et al. (2007). All these studies tend to show that gravitation might play an important role in the collimation and structure formation of relativistic jets, independently of the action of the large-scale magnetic fields usually invoked.

Besides the explicit integration of the equations of motion, in this work we analyze the vortical orbits in STVG. Specifically, we adapt the conditions of de Felice & Calvani (1972) for vortical orbits to the modified equation of motion (20). Defining:

$$\Gamma = \frac{E^2}{c^4} - m^2, \quad (28)$$

the vortical orbits in STVG are the trajectories that satisfy:

$$\Gamma > 0, \quad (29)$$

$$-a^2\Gamma \leq \mathcal{Q} + L^2 \leq a^2\Gamma, \quad (30)$$

$$L^2 + \mathcal{Q} \leq L^2 \leq \frac{(a^2\Gamma + L^2 + \mathcal{Q})^2}{4a^2\Gamma}. \quad (31)$$

By varying the initial parameters of the particle, and the free parameters of STVG, we explore the amount of vortical orbits in the theory. Then, we compare the results with GR. According to the mentioned line of research, a large number of vortical orbits is convenient since they are the starting point for explaining collimation and acceleration in axially symmetric spacetimes.

#### 4 NUMERICAL TREATMENT

We integrate the first order equations for the particle coordinates (19)-(22) numerically. We carefully select a reasonable set of values for the initial conditions. Specifically,

(i) We fix the spacetime geometry and the fields on it by setting  $M$ ,  $a$  and  $\alpha$ . In order to find acceptable values for  $\alpha$  we appeal to the parameter  $M_0$ , studied extensively by Moffat; see for instance Brownstein & Moffat (2006) and Brownstein & Moffat (2007). These parameters are related by:

$$\alpha = \sqrt{\frac{M_0}{M}}. \quad (32)$$

(ii) We set the particle properties:  $m, \kappa$ , and the initial position in Boyer-Lindquist coordinates  $r_0, \theta_0, \phi_0$ . Without loss of generality, we set  $\phi_0 = 0$ , locating initially the particle on the  $x - z$  plane.

(iii) We fix the initial four momentum  $p^\mu = dx^\mu/d\lambda$  of the particle. Since we are interested on the effects of gravito-magnetic forces, we set initially  $p_\phi = 0$ .

(iv) For the  $t$ -component of momentum we have:

$$p_t = -mc\gamma\sqrt{g_{tt}}, \quad (33)$$

where  $\gamma$  is the local Lorentz factor of the particle.

(v) The initial values of the components  $p_r, p_\theta$  require further steps because they depend on the ejection angle  $\theta_{ej}$  of the particle spatial velocity with the  $z$ -axis. It is convenient to work initially in Kerr-Schild coordinates. We set  $\theta_{ej}$  and solve the system of non-linear equations for the Kerr-Schild momentum components  $\tilde{p}_x, \tilde{p}_z$ :

$$\cos \theta_{ej} = \frac{\tilde{p}^i z^j g_{ij}}{\sqrt{\tilde{p}^i \tilde{p}_i} \sqrt{z^i z_i}}, \quad (34)$$

$$\tilde{p}^\mu \tilde{p}_\mu = -m^2 c^2, \quad (35)$$

where  $i = 1, 2, 3$ , and  $z^i = (0, 0, 1)$ . Setting  $\tilde{p}_y = 0$  for the same reason we set  $p_\phi = 0$ , and taking  $p_t$  from Eq. (33), we solve the non-linear system applying a Newton-Raphson subroutine that we take from Press et al. (1992). After finding the roots  $\tilde{p}_x, \tilde{p}_z$ , we obtain the initial Boyer-Lindquist components  $p_r, p_\theta$  from a direct change of coordinates.

(vi) With the four-momentum at the initial time, we calculate the constants of motion for the particle movement:

$$E = -p_t c - qA_t, \quad (36)$$

$$L = p_\phi + qA_\phi, \quad (37)$$

and  $\mathcal{K}, \mathcal{Q}$  as given by (26), (27), respectively. The mass of the particle is the fourth independent constant of motion, that we calculate as a check for consistency:

$$m = \sqrt{\frac{-p^\mu p_\mu}{c^2}}. \quad (38)$$

(vii) Once the initial conditions are settled, we proceed to integrate Eqs. (19)-(22) numerically. We apply a fourth order Runge-Kutta subroutine taken from Press et al. (1992). Along the run we calculate the local Lorentz factor  $\gamma$  as measured by a Zero Angular Momentum Observer with four velocity  $u_\mu \rightarrow (u_t, \vec{0})$ , based on the expression of Crawford & Tereno (2002) for physical velocities.

#### 5 RESULTS

We apply the numerical code described in the previous Section to the rapid spinning supermassive black hole in M87. We set the mass to  $M = 6 \times 10^9 M_\odot$  and the angular momentum to  $a = 0.9 G_N M/c$ , as estimated by Gebhardt et al. (2011), and Li et al. (2009), respectively.

From observations reported in Broderick et al. (2015), we know that M87\* radius is at most  $8 G_N M/c^2$ . This implies an upper limit for the parameter  $M_0$ , and correspondingly for  $\alpha$ . We find the upper limit:

$$M_0 \lesssim 10^{11} M_\odot. \quad (39)$$

In the first run, we compare results with  $M_0 = 10^{10} M_\odot, 10^{11} M_\odot$  and  $10^{12} M_\odot$ . The latter violates restriction (39) but we include it for consistency checks. We place a test particle with mass  $m = 1g$  at  $r_0 = 140 G_N M/c^2, \theta_0 = 0.18, \phi_0 = 0$ . We set the initial Lorentz factor to  $\gamma = 2$ . Such parameters are based on recent observational results Mertens et al. (2016). For the parameter  $\kappa$  we first use Moffat's prescription  $\kappa = \sqrt{\alpha G_N}$ , and then explore further values. We set an ejection angle  $\theta_{ej} = 0$ , i. e. the particle is ejected along the direction  $\hat{z}$ .

In Fig. 4 (left) we display the initial velocity of the particle and the initial gravito-magnetic field. Fig. 4 (right)



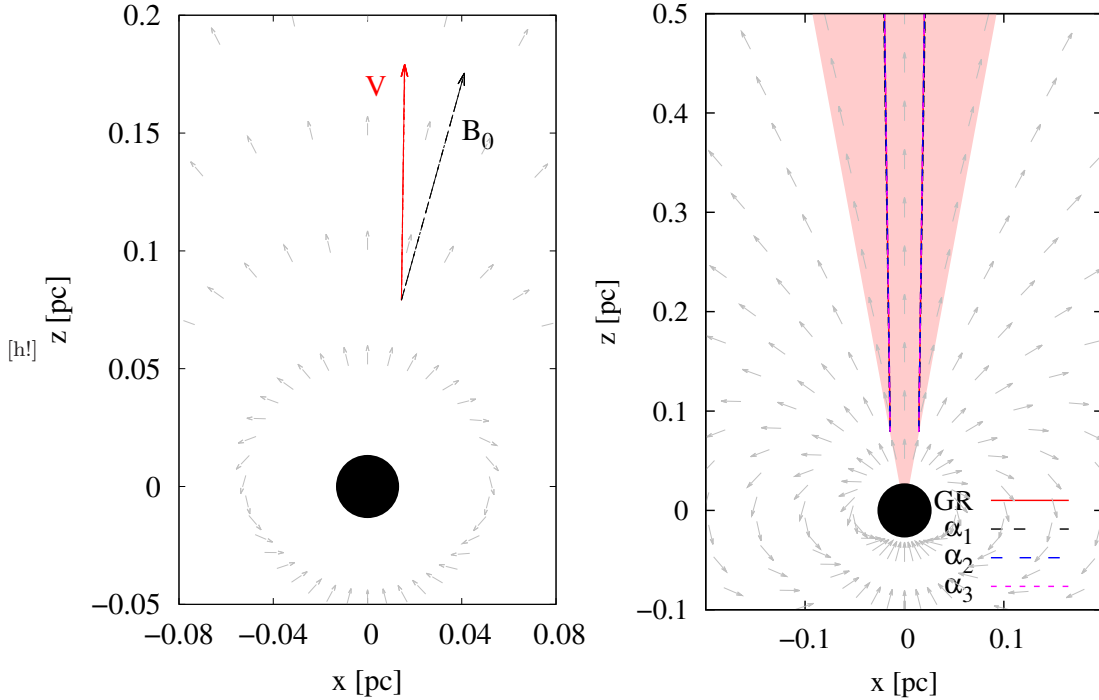


**Figure 4.** *Left:* Initial velocity of the particle, along with the gravito-magnetic field at the particle initial position. From the relative position of both vectors, the initial gravito-magnetic force is  $\vec{\phi}$  directed. *Right:* Projection of the particle trajectories on the  $x - z$  plane for distinct values of  $\alpha$ . Deviations from GR predictions are negligible. The filled region indicates the relativistic jet of M87\*, with the opening angle  $\Theta \sim 0.18$ , as determined from observations.

shows the trajectories of the particle on the  $x - z$  plane for the distinct values of  $\alpha$ . As we can see, deviations from GR are negligible. The filled region shown in Fig. 4 (*right*) is the relativistic jet of M87\*, with the opening angle  $\Theta \sim 0.18$ , determined from direct observation (see Mertens et al. 2016).

Although the trajectories are very similar, we find large deviations from GR on the kinematic properties of the particle. In Fig. 5 (*top*) we plot the radial coordinate  $r$  of the particle as a function of the time coordinate  $t$ . We find that, contrarily to what happens in the weak field limit, STVG is not equivalent to GR regarding the radial motion near the source. When we increase the parameter  $\alpha$ , repulsion and attraction grow in equal proportion, but STVG equations are not linear and attraction prevails because the black hole energy also increases with  $\alpha$ . This effect can also be seen from the local Lorentz factor  $\gamma$  of the particle. In Fig. 5 (*bottom*) we plot  $\gamma$  as a function of  $t$ ; we find that the decrement of  $\gamma$  is deeper for larger  $\alpha$ .

Concerning the motion in the coordinate  $\phi$ , the angular velocity  $\omega_\phi$  increases with  $\alpha$ . However we do not associate such effect with Lorentz-like forces, but with the enhanced frame dragging due to the larger black hole energy. In this model, Lorentz-like forces are negligible because of the smallness of the  $\kappa$  parameter. In the following, we explore further values of  $\kappa$ .

In the second run, we fix  $M_0 = 10^{11} M_\odot$  and sample the values  $\kappa = 10^2 \sqrt{\alpha G_N}$ ,  $10^3 \sqrt{\alpha G_N}$ , and  $10^4 \sqrt{\alpha G_N}$ . Increasing  $\kappa$  enhances Lorentz-like effects, while keeps the geometry fixed.

Abandoning Moffat’s prescription for  $\kappa$  may lead to problems in retrieving the weak field equation (1). However,

the theory is still being explored, and this outcomes give us insights into future research directions. For instance, abandoning the constant approximation of the scalar field  $G$  and including scale dependence.

We explore the predictions of STVG for two different values of the ejection angle of the particles:  $\theta_{ej} = 0$  and  $0.3$ . In Fig. 6 we show the initial configuration of the velocity and the gravito-magnetic field for such systems. In the first case the particle moves in the region A of Fig. 3, while for the second case on region B. Because of gravito-magnetic forces, we expect angular velocities  $\omega_\phi$  with opposite signs in each region. Regarding the equation of motion (20) for  $\theta$ , we choose the sign  $-$  for case A and  $+$  for B.

In Fig. 7 we show the angular velocity  $\omega_\phi$ , defined as the quotient between  $d\phi/d\lambda$  and  $dt/d\lambda$ , for cases A and B as a function of the coordinate  $z$ . We find significant deviations from GR. In case A,  $\phi$  rotation is enhanced by the gravito-magnetic field force, leading to higher maxima, parametrized by  $\kappa$ . The rapid decay of  $\omega_\phi$  for larger  $\kappa$  is related to the movement of the particle in  $\theta$ , as we explain below. For case B, we obtain initially negative values for  $\omega_\phi$ . This is because the initial gravito-magnetic force is directed towards  $-\vec{\phi}$ . Along the particle trajectory the dipole field lines rotate, changing their disposition with respect to the particle velocity, and leading to “case A” configurations. Consequently, the gravito-magnetic forces change their sign, and  $\omega_\phi$  grows for larger  $z$ .

In Fig. 8 we plot the  $x - z$  trajectories for both cases and the mentioned values of  $\kappa$ . Again, we find significant deviations from GR predictions. Deflection in  $\theta$  can be explained as a second order effect of the Lorentz-like force that acts on the particle when it accelerates in the  $\vec{\phi}$  direction. In case A,

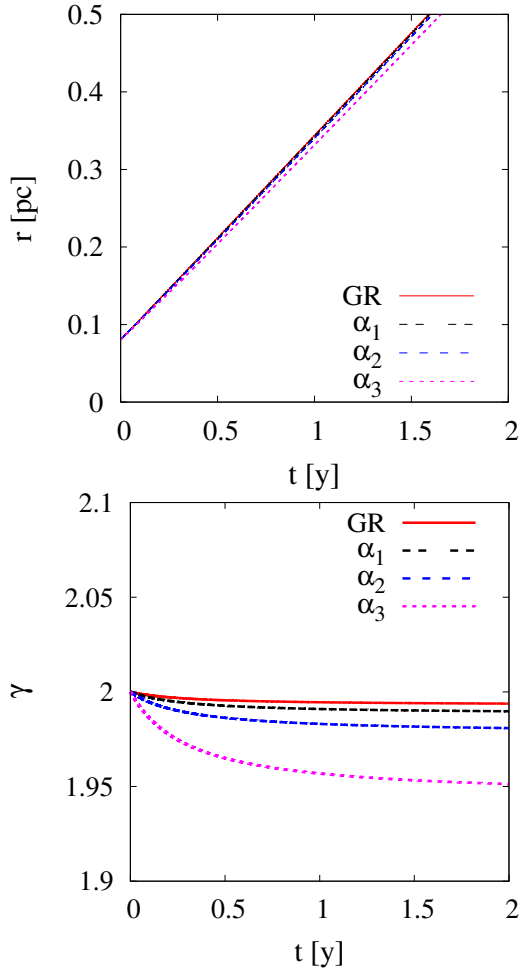


**Figure 5.** *Top:* Radial coordinate  $r$  as a function of time coordinate  $t$  for different values of the parameter  $\alpha$ . *Bottom:* Local Lorentz factor  $\gamma$  of the particle as a function of the time coordinate  $t$ . The value of  $\gamma$  decreases deeper for larger values of  $\alpha$ .

the particle deviates from the rotational axis, resulting in a wider relativistic jet. On the contrary, in case *B* the particle trajectory deviates towards the rotational axis, contributing to jet collimation. In these figures, as before, the filled region represents the relativistic jet of M87. In both cases the deviation in  $\theta$  leads to a quick alignment of the particle velocity with the field lines, canceling out gravito-magnetic forces. This is the reason of the rapid decay of  $\omega_\phi$  for larger  $\kappa$  in Fig. 7.

The enhancement of Lorentz-like forces with increasing  $\kappa$  is also reflected on the kinematic properties of the particle. Since gravito-electrical repulsion increases, the particle moves away even faster than in GR. This can be seen from Fig. 9 (*top*) where we plot the radial coordinate  $r$  as a function of the time coordinate  $t$  for particles. Furthermore, from Fig. 9 (*bottom*) we notice that the local Lorentz factor  $\gamma$  grows significantly with time and reaches high values. Then, in this strong field regime, the particle is gravitationally accelerating. This can be used to invoke an active role of gravity in jet formation (see our discussion in Section 6).

Finally, we use our code for studying the number of vortical orbits in STVG. We vary the initial angle  $\theta_0$ , and the ejection angle  $\theta_{ej}$ , and test whether the resulting trajectories

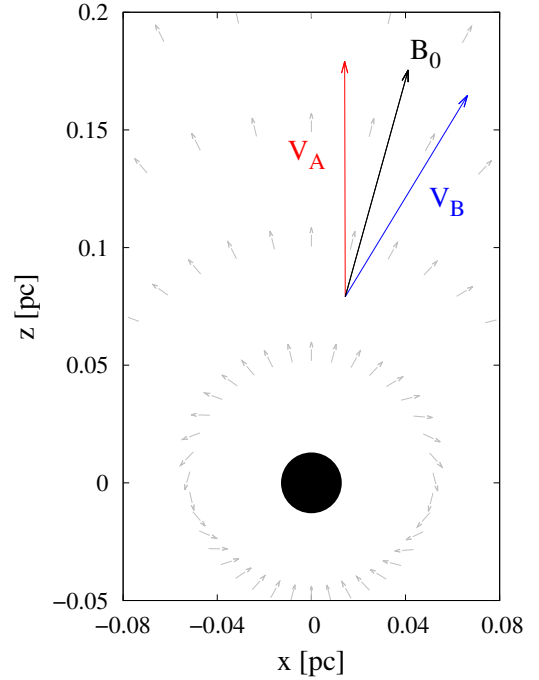


**Figure 6.** Initial configuration of the particles velocities and the gravito-magnetic field for case A and B. Because of gravito-magnetic forces, we expect opposite signs for the angular velocity  $\omega_\phi$  in each case.

satisfy the vortical conditions (29)-(31). In Fig. 10 we plot the parameter space  $\theta_0 - \theta_{ej}$ , and fill the regions that include vortical orbits. As we can see, the number of vortical orbits grows with  $\kappa$ . This occurs because of gravito-magnetic forces that lead to a better collimation, or because the enhancement of gravitational repulsion. Future work will be devoted to the analysis and perturbation of such orbits.

All these results show that STVG theory has huge impact on relativistic jet physics. In the next section, we discuss some interesting applications to jet phenomenology.

## 6 DISCUSSION

We have studied trajectories of particles in STVG-Kerr geometry. We find that STVG is not equivalent to GR in the strong field regime. In the face of current problems of jet formation models, some STVG predictions seem attractive. The case of M87 and its jets is particularly interesting, since the jet has been recently resolved on scales of 100-1000 Schwarzschild radii (Mertens et al. 2016). Very Long Base Line radio observations at 43 GHz have revealed a jet that initially expands with a parabolic profile (Asada & Nakamura 2012) and then transits to a conical jet at a projected distance of  $\sim 350$  mas ( $2 \text{ mas} \approx 0.16 \text{ pc}$ ). The radius of the jet evolves with the distance to the central source as  $r_{jet} \propto z^{0.6}$ , with significant oscillations that might reflect the growing of Kelvin-Helmholtz instabilities. The observations reveal the existence of a structured jet, with clear stratification: a slow, outer component and a faster relativistic spine (Mertens et al. 2016). Such structure is consistent with the gravitational acceleration discussed in the previous section. In STVG-Kerr spacetime vortical particles close to the jet

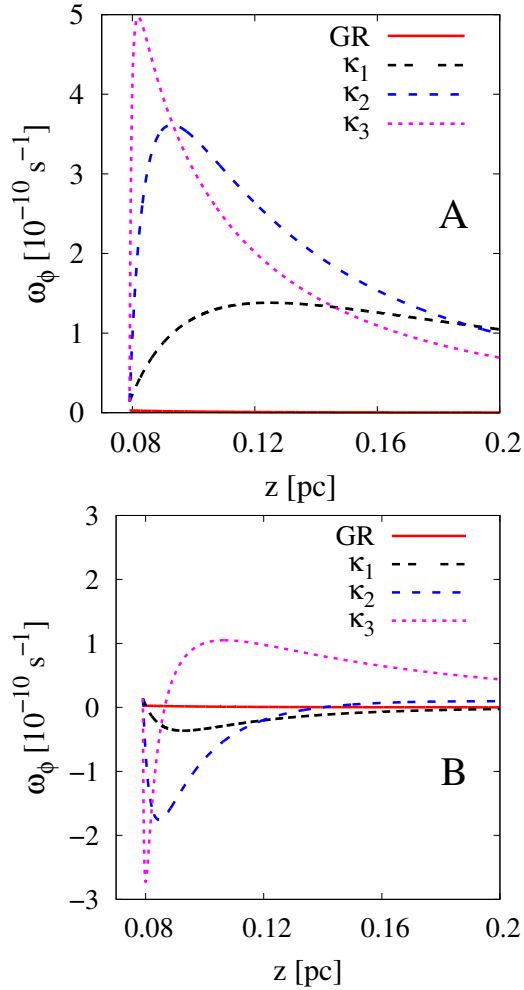


**Figure 7.** *Top:* Angular velocity  $\omega_\phi$  as a function of the  $z$ -coordinate for the initial velocity of case A. The angular velocity maximum grows with  $\kappa$  as a consequence of the gravito-magnetic force enhancement. The rapid decay happens because, for larger  $\kappa$ , the particle deviates in the  $\theta$  direction, getting aligned with the field lines. *Bottom:* Angular velocity  $\omega_\phi$  as a function of the  $z$ -coordinate for the initial velocity of case B. Initially,  $\omega_\phi$  is negative because of the relative disposition of the gravito-magnetic field lines and the particle velocity. Minima are deeper for larger  $\kappa$  because the Lorentz-like force increases. As  $z$  grows, the gravito-magnetic field lines rotate giving raise to “case A” configurations and, consequently, produce an increment of the angular velocity  $\omega_\phi$ .

axis are accelerating and move faster in the  $z$ -direction than the outer particles, leading naturally to the jet with a fast spine. This feature has been suggested to be common among extragalactic jets (Sol et al. 1989).

The jet of M87 is also the first one where rotation has been directly observed. The jet first rotates clockwise and then the outer components rotates counterclockwise. Assuming conservations of the specific energy and angular momentum and Keplerian motion in the accretion disks, allows to infer a rotation angular velocity of  $\omega_\phi \sim 10^{-6} \text{ s}^{-1}$  (Mertens et al. 2016).

Since at the launching region the effects of gravitational gravito-magnetic forces are critical, this rotation might result from gravitational forces in the STVG scenario. In order

to check the viability of this conjecture, we run our code to study the near black hole region, adopting  $r_0 = 5R_S$ ,  $M_0 = 10^{10} M_\odot$ ,  $\kappa = 10^1 \sqrt{\alpha G_N}$ ,  $10^2 \sqrt{\alpha G_N}$ ,  $10^3 \sqrt{\alpha G_N}$ , and a wide ejection angle, as expected from the Blandford-Payne mechanism for jet launching (Blandford & Payne 1982; Spruit 2010). The initial disposition of the gravito-magnetic field and the velocity of the particle can be seen in Fig. 11 (left). The  $x - z$  trajectories obtained for different values of  $\kappa$  are shown in Fig. 11 (right). The filled region in the latter figure is the jet, as observed and parametrized by Mertens et al. (2016). Again, we notice how gravito-magnetic forces contribute to the collimation of the jet.

The initial gravito-magnetic force on the particle leads to counter-rotation in  $\phi$ . But, as we mentioned in the previous section, the field lines rotate along the trajectory. Then, from a certain  $z$ , the sign of gravito-magnetic forces change, and  $\omega_\phi$  starts growing. The behavior of  $\omega_\phi$  as a function of  $z$  can be seen from Fig. 12, for different values of  $\kappa$ . The inversion of the jet rotation, and the order of magnitude for  $\omega_\phi$ , are consistent with Mertens et al. (2016) observational and modeling results. Rotations of the order of  $10^{-6} \text{ s}^{-1}$  can be achieved by gravitational effects only in STVG gravity.

Conditions for strong jet collimation in the standard magnetic jet model contradict with conditions of strong initial acceleration, since they require distinct inclination angles for the magnetic field lines. Collimation might be produced by some external agent. In Spruit et al. (1997) a collimation mechanism based on a dipole-like magnetic field is proposed. The gravito-magnetic field of STVG is independent of the magnetic field, and may serve as the external collimating agent as well.

In summary, current observations of extragalactic jets are compatible with STVG for moderate values of the  $\kappa$  parameter ( $\sim 10^2 \sqrt{\alpha G_N}$ ). Further observations of the innermost region can impose more stringent constraints.

## 7 CONCLUSIONS

We applied the STVG theory with constant scalar fields and  $\tilde{\mu} = 0$  approximation to M87\*. The approximation adopted for  $\tilde{\mu}$  is justified because its effects manifest at kiloparsec scales from the gravitational source, and we are interested on sub-parsec astrophysical structures. We found a resemblance of this regime with Einstein-Maxwell formalism.

We described the STVG-Kerr spacetime. The black hole event horizon and ergosphere grow in size with the free parameter  $\alpha$  of the theory. Since there are constraints on the size of M87\* from mm-VLBI observations, we set an upper limit for the related parameter  $M_0$ , in this mass range.

Unlike many current gravitational theories, STVG is not purely geometrical. The theory assumes the existence of a Yukawa-type vector field  $\phi^\mu$  that couples to matter. We characterized the effects of such vector field on the trajectories of test particles in STVG-Kerr spacetime. Repulsive gravito-electrical components counteracts enhanced attraction and serves to recover classical limits; gravito-magnetic components are dipole-like and its effects are novel predictions of STVG.

We derived the equations of motion for a test particle with mass  $m$  in STVG-Kerr spacetime. The equations depend on the coupling constant  $\kappa$ . Moffat proposed the value



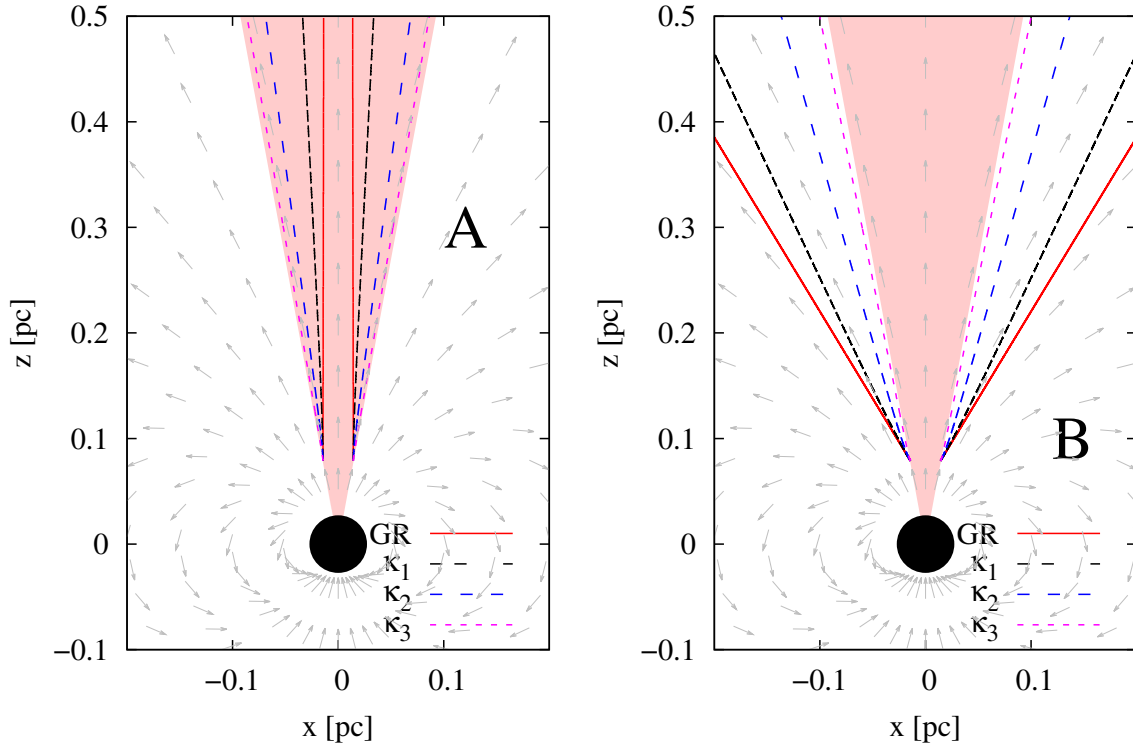


**Figure 8.** *Left:*  $x - z$  projection of trajectories in case A for distinct values of  $\kappa$ . We find deflection along  $\theta$  as a gravito-magnetic second order effect. The filled region represents the sub-parsec relativistic jet of M87. *Right:*  $x - z$  projection of case B trajectories for distinct values of  $\kappa$ . Gravito-magnetic forces contribute to jet collimation, deviating the particle towards the rotation axis.

$\kappa = \sqrt{\alpha G_N}$  for recovering the correct weak field acceleration, but such choice works on a constant scalar field approximation for  $G_\infty$ . We treated instead  $\kappa$  as a free parameter to study its effects on particle motion, and to gain insight into abandoning the constant scalar field approximation for  $G_\infty$ .

We developed a code for integrating the equations of motion for a particle in a relativistic jet. Initially we varied the parameter  $\alpha$ , adopting the prescription of Moffat for  $\kappa$ . The effects of vector forces resulted negligible, but the increase of the black hole energy with  $\alpha$  led to a deep decrease of the particle velocity, as compared with GR. We conclude that STVG differs with GR not only far from the gravitational source, where phenomena associated with dark matter happen, but also in the strong field regime near the source.

Then, we fixed the parameter  $\alpha$  and increased the coupling constant  $\kappa$  a few orders of magnitude. The effects of vector forces clearly arose. Because of gravito-electrical repulsion, the particles accelerate and reach high Lorentz factors. As expected, gravito-magnetic forces influenced the angular velocity  $\omega_\phi$ , depending critically on the initial direction of the particle velocity. As a second order effect, we found collimation and de-collimation in the coordinate  $\theta$ , depending on the initial velocity.

Independently, we begin a semi-analytical study of vortical orbits in STVG-Kerr spacetime. We find that STVG includes a larger number of vortical orbits than GR, for increasing  $\kappa$ . This means that the theory is more suitable for modeling some jet phenomena. Future work will be devoted to reproduce and compare GR results with STVG following this line of research in more detail.

Finally, we compared observational and modeling re-

sults about the formation zone of the jet of M87, with predictions of STVG. We conclude that gravitation might play an important role in the process of acceleration and collimation of the jet. Interestingly enough, we found that the observed rotation and counter-rotation of M87\* jet could be a consequence of the gravito-magnetic field.

## ACKNOWLEDGEMENTS

This work was supported by grants AYA2016-76012-C3-1-P (Ministro de Educación, Cultura y Deporte, España) and PIP 0338 (CONICET, Argentina). We would like to thank Luciano Combi, and Santiago del Palacio, for helpful discussions.

## REFERENCES

- Agnese R., et al., 2014, *Physical Review Letters*, **112**, 241302
- Aprile E., et al., 2012, *Physical Review Letters*, **109**, 181301
- Asada K., Nakamura M., 2012, *ApJ*, **745**, L28
- Babcock H. W., 1939, *Lick Observatory Bulletin*, **19**, 41
- Blandford R. D., Payne D. G., 1982, *MNRAS*, **199**, 883
- Broderick A. E., Narayan R., Kormendy J., Perlman E. S., Rieke M. J., Doeleman S. S., 2015, *ApJ*, **805**, 179
- Brownstein J. R., Moffat J. W., 2006, *The Astrophysical Journal*, **636**, 721
- Brownstein J. R., Moffat J. W., 2007, *MNRAS*, **382**, 29
- Carter B., 1968, *Phys. Rev.*, **174**, 1559
- Crawford P., Tereno I., 2002, *General Relativity and Gravitation*, **34**, 2075
- Famaey B., McGaugh S. S., 2012, *Living Reviews in Relativity*, **15**, 10

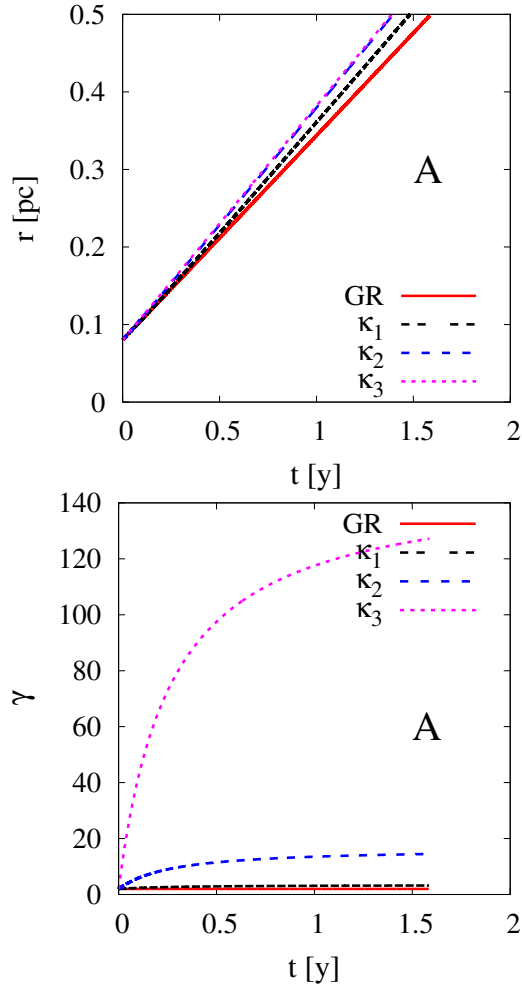


**Figure 9.** *Top:* Radial coordinate  $r$  as a function of the time coordinate  $t$  for particles in case A. The particles move faster in the radial direction because of the enhancement of the repulsive gravito-electric force with growing  $\kappa$ . *Bottom:* Local Lorentz factor  $\gamma$  for particles in case A as a function of time coordinate  $t$ . The enhancement of repulsive gravito-electric forces with larger  $\kappa$  manifests in  $\gamma$ , growing up to high values. We find similar behaviors for particles in case B.

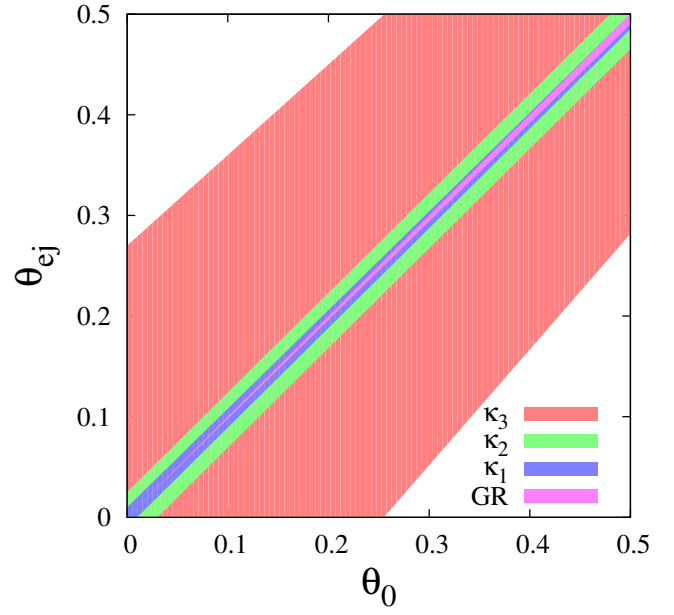


**Figure 10.** Parameter space  $\theta_0 - \theta_{ej}$ , with vortical orbits regions filled. Compared with GR, increasing  $\kappa$  turns trajectories in vortical orbits. In this sense, STVG is more suitable than GR for explaining jet formation processes.

1992, Numerical Recipes in Fortran 77: The Art of Scientific Computing, 2nd edn. Cambridge University Press  
 Sol H., Pelletier G., Asseo E., 1989, *MNRAS*, **237**, 411  
 Spruit H. C., 2010, in Belloni T., ed., Lecture Notes in Physics, Berlin Springer Verlag Vol. 794, Lecture Notes in Physics, Berlin Springer Verlag. p. 233 ([arXiv:0804.3096](https://arxiv.org/abs/0804.3096)), doi:10.1007/978-3-540-76937-8\_9  
 Spruit H. C., Foglizzo T., Stehle R., 1997, *MNRAS*, **288**, 333  
 de Felice F., Calvani M., 1972, Nuovo Cimento B Serie, **10**, 447  
 de Felice F., Curir A., 1992, *Classical and Quantum Gravity*, **9**, 1303

This paper has been typeset from a  $\text{\LaTeX}$  file prepared by the author.

Gariel J., MacCallum M. A. H., Marcilhacy G., Santos N. O., 2007, ArXiv General Relativity and Quantum Cosmology e-prints,  
 Gebhardt K., Adams J., Richstone D., Lauer T. R., Faber S. M., Gültekin K., Murphy J., Tremaine S., 2011, *ApJ*, **729**, 119  
 Hussain S., Jamil M., 2015, *Phys. Rev. D*, **92**, 043008  
 LUX Collaboration et al., 2013, preprint, ([arXiv:1310.8214](https://arxiv.org/abs/1310.8214))  
 Li Y.-R., Yuan Y.-F., Wang J.-M., Wang J.-C., Zhang S., 2009, The Astrophysical Journal, 699, 513  
 Mertens F., Lobanov A. P., Walker R. C., Hardee P. E., 2016, *A&A*, **595**, A54  
 Milgrom M., 1983, *ApJ*, **270**, 365  
 Misner C., Thorne K., Wheeler J., 1973, Gravitation. W. H. Freeman  
 Moffat J. W., 2006, Journal of Cosmology and Astroparticle Physics, 2006, 004  
 Moffat J. W., 2015, *European Physical Journal C*, **75**, 175  
 Moffat J. W., Rahvar S., 2013, *MNRAS*, **436**, 1439  
 Moffat J. W., Rahvar S., 2014, *MNRAS*, **441**, 3724  
 Moffat J. W., Toth V. T., 2007, preprint, ([arXiv:0710.0364](https://arxiv.org/abs/0710.0364))  
 Press W. H., Teukolsky S. A., Vetterling W. T., Flannery B. P.,

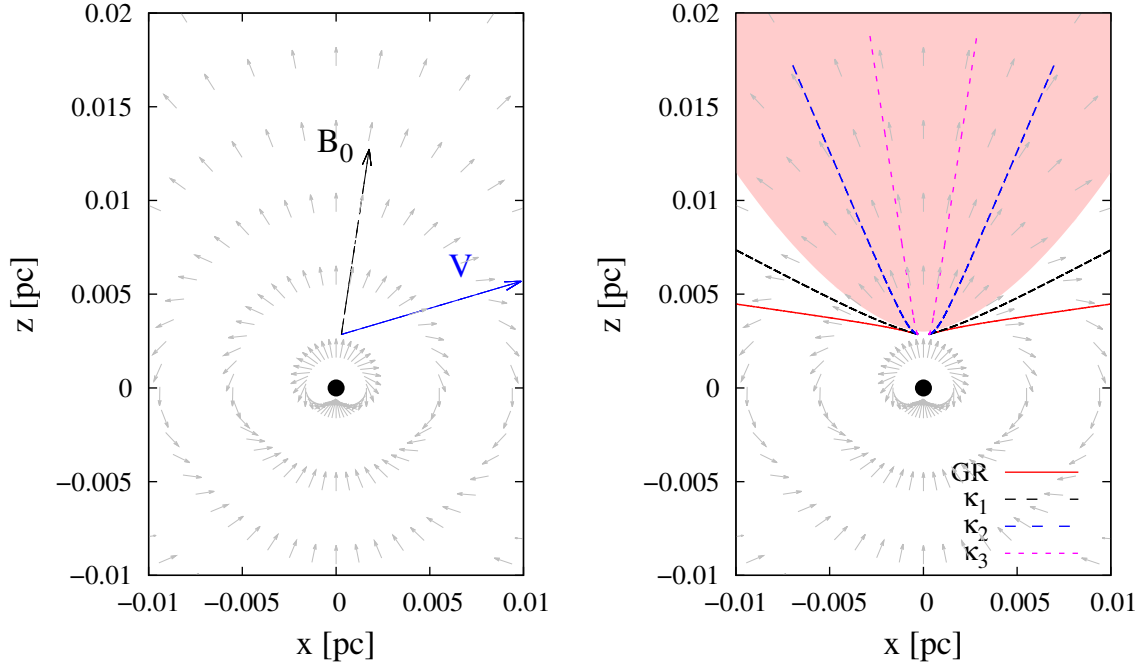


**Figure 11.** *Left:* Initial configuration of the particle velocity and the gravito-magnetic field at the launching region. *Right:*  $x-z$  projection of the trajectories of the particle, for different values of  $\kappa$ . The filled region is the launched jet. Gravito-magnetic forces contribute to the collimation of the jet.

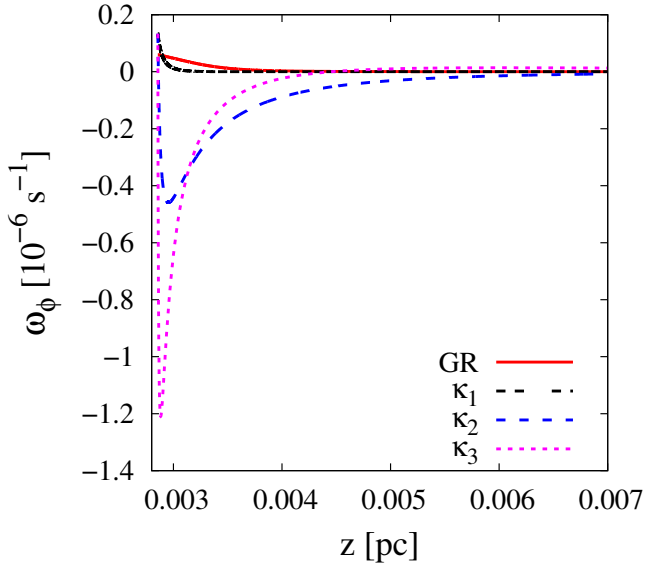


**Figure 12.** Angular velocity  $\omega_\phi$  for a particle ejected with a wide angle, near the black hole event horizon. The behavior of  $\omega_\phi$  is related to the disposition of the gravito-magnetic field and the velocity of the particle, along the trajectory.